PAPER • OPEN ACCESS

Multi-bit operations in vertical spintronic shift registers

View the article online for updates and enhancements.

Related content

- Systematic layer-by-layer characterization of multilayers for three-dimensional data storage and logic
  Dorothée Petit, Reinoud Lavrijsen, JiHyun Lee et al.

- A magnetic shift register with out-of-plane magnetized layers
  R Mansell, A Beguivin, A Fernández-Pacheco et al.

- Topical Review
  A O Adeyeye and N Singh

Recent citations

- Intra-wire coupling in segmented Ni/Cu nanowires deposited by electrodeposition
  Philip Sergelius *et al*

- A magnetic shift register with out-of-plane magnetized layers
  R Mansell *et al*

- Vector magnetometry of Fe/Cr/Fe trilayers with biquadratic coupling
  R Mansell *et al*

IOP ebooks™

Bringing you innovative digital publishing with leading voices to create your essential collection of books in STEM research.

Start exploring the collection - download the first chapter of every title for free.

Multi-bit operations in vertical spintronic shift registers

Reinoud Lavrijsen[1]**, Dorothée C M C Petit, Amalio Fernández-Pacheco, JiHyun Lee, Rhodri Mansell and Russell P Cowburn**

Thin Film Magnetism Group, Cavendish Laboratory, University of Cambridge, JJ Thomson Avenue, Cambridge, CB3 0HE, UK

E-mail: r.lavrijsen@tue.nl

Abstract

Spintronic devices have in general demonstrated the feasibility of non-volatile memory storage and simple Boolean logic operations. Modern microprocessors have one further frequently used digital operation: bit-wise operations on multiple bits simultaneously. Such operations are important for binary multiplication and division and in efficient microprocessor architectures such as reduced instruction set computing (RISC). In this paper we show a four-stage vertical serial shift register made from RKKY coupled ultrathin (0.9 nm) perpendicularly magnetised layers into which a 3-bit data word is injected. The entire four stage shift register occupies a total length (thickness) of only 16 nm. We show how under the action of an externally applied magnetic field bits can be shifted together as a word and then manipulated individually, including being brought together to perform logic operations. This is one of the highest level demonstrations of logic operation ever performed on data in the magnetic state and brings closer the possibility of ultrahigh density all-magnetic microprocessors.

Keywords: spintronics, nano-scale shift register, magnetic logic, magnetic kink soliton, perpendicular

S Online supplementary data available from stacks.iop.org/Nano/25/105201/mmedia

(Some figures may appear in colour only in the online journal)

1. Introduction

The progress of spintronics and nano-magnetic logic to effectively use the third dimension, more specifically the space above the two-dimensional wafer plane, has been impeded by the added process complexity [1–5]. Challenging 3D device concepts have been proposed but progress towards full three-dimensional functionality is slow [6, 7]. We recently demonstrated a simple magnetic kink soliton [8, 9] ratchet which actively uses the third dimension [10]. Here the term 'kink soliton' is used to refer to the spatially localised boundary between two anti-parallel magnetic domains [8, 11]. In our particular case, a soliton is formed by two layers pointing in the same direction, and it is referred to as sharp as it does not involve any further layers. This concept could be used to boost the performance of future three-dimensional spintronic data-storage, memory, or logic devices [1, 5–7, 12, 13]. Specifically, we demonstrated a shift register in which a sharp magnetic soliton was propagated vertically, unidirectionally and synchronously with a magnetic field. We used a superlattice (SL) consisting of ultrathin perpendicularly magnetized Pt/CoFeB/Pt layers coupled antiferromagnetically through Ru using the Ruderman–Kittel–Kasuya–Yosida (RKKY)-mechanism [14–20]. Here we show how multiple solitons can be injected, propagated and annihilated to show full serial shift register potential [21, 22] and how we can perform logic operations using sharp magnetic kink solitons in a single SL based on ultrathin Pt/Co layers.

[1] Present address: Eindhoven University of Technology, Den Dolech 2, 5612 AZ Eindhoven, The Netherlands
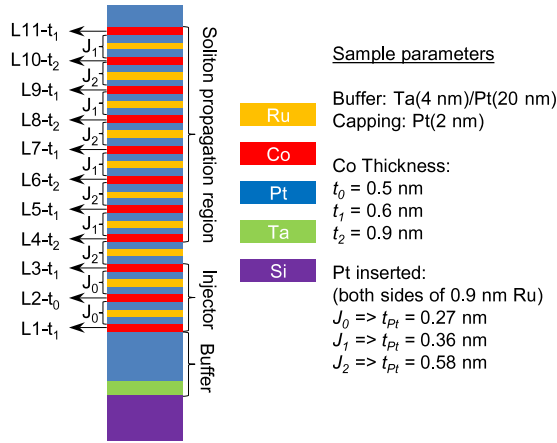
Figure 1. Schematic illustration of the SL sample and its structural parameters.

2. Sample and experimental

The SL studied here is formed by non-patterned continuous films, the layer structure and parameters are given figure 1. The SL consists of 44 layers with a total thickness of ∼51 nm, of which 11 layers are ferromagnetic (FM) Co with different thicknesses ($t_0 = 0.5$ nm, $t_1 = 0.6$ nm and $t_2 = 0.9$ nm). The SL is grown on a buffer layer of Ta(4 nm)/Pt(20 nm) and capped with a 2 nm Pt layer. The FM Co layers are antiferromagnetically coupled to their neighbors through Pt/Ru(0.9 nm)/Pt spacers by the RKKY mechanism [17]. The inserted Pt thickness at the interfaces between Co and Ru are varied to set the coupling strength J_0, J_1 and J_2 [17]. The bottom three layers of the stack are from now on referred to as the injector and the top eight layers as the soliton propagation region. The alternating coupling strengths J_1, J_2 and FM layer thicknesses t_1, t_2 in the soliton propagation region induces an upward ratchet for solitons as explained in [10]. Note that in contrast to our previous report, we now use perpendicularly magnetized Pt/Co layers with a higher coercivity compared to Pt/CoFeB [23]. Using Pt/Co allows us to inject multiple solitons into the SL as we will explain later.

3. Results

3.1. Major hysteresis loop

In figure 2(a) we show the major hysteresis loop measured using a vibrating sample magnetometer (VSM). The VSM signal is directly proportional to the magnetic moment of the sample. All VSM data presented are obtained by subtracting the diamagnetic background of the Si substrate measured at applied fields >10 kOe (see inset graph at bottom right corner of figure 2(b)). The VSM data allows us to determine if a t_0, t_1 or t_2 layer has switched since we know the fraction of material in every layer (see top left text inset of figure 2(a)). This allows us to determine the configuration of the SL after every transition in the hysteresis loop. This is schematically illustrated in figure 2(b) where the numbered balloons refer to the corresponding plateau in the signal shown in (a). A dotted outline indicates which layer has switched
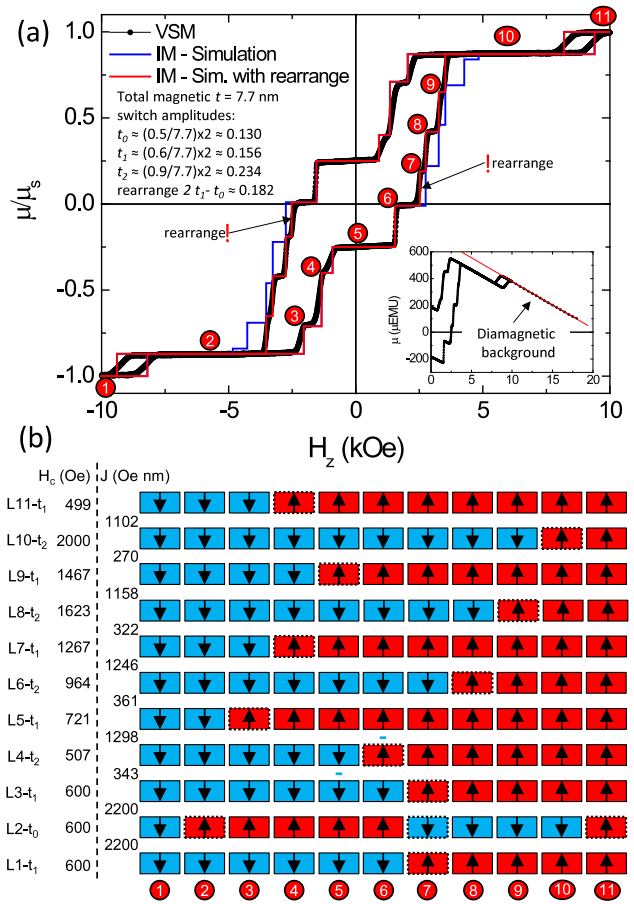

Figure 2. Major hysteresis loop and the derived configurations of the SL. (a) Major hysteresis loops obtained by VSM. The rearrange transitions in the IM model are indicated by the exclamation marks. The top left text inset calculates the fractional signal of transitions as used in (b). The bottom right inset graph shows the raw VSM signal showing the subtracted background signal. (b) Schematically illustration of the magnetic configuration of the SL corresponding to the numbered balloons at every plateau in the hysteresis loops in (a). The parameters J between the layers and the H_c of the layers used for the IM model are listed to the left of the schematic in (b).

compared to the previous configuration. In the supplementary information (available at stacks.iop.org/Nano/25/105201/m media) we supply supporting evidence for this switching sequence using the magneto optical-Kerr effect (MOKE).

We can simulate the major VSM hysteresis loop using a simple Ising-macrospin (IM) model using the following input parameters: the coercivity of every layer at room temperature (H_c), the coupling between layers (J) and thickness of the layers (t) [10]. Note that in this simple model the temperature effects are captured by the H_c parameter. The coupling strength J is for convenience expressed in units of magnetic field times length since the RKKY coupling between two FM layers is a surface term and scales with the thickness of the FM layer. The switching field H_s of a layer can then be calculated using $H_s = H_c + J_{tot}/t$ and J_{tot} is the sum of the couplings experienced by the layer considered from its nearest neighbors. For convenience we use $J > 0$ for antiferromagnetic coupling.

The blue solid line in figure 2(a) is simulated with the IM model using the parameters as listed left to the schematic

SL illustration in figure 2(b). These parameters are extracted by systematically measuring switching transitions in different configurations of the SL similar to the data described in figures 3–5, the exact procedure will be published elsewhere. The bottom three layers of the SL have a relatively higher coupling J_0 compared to the rest of the SL. This allows us to inject solitons between L3 and L4 (indicated by the blue minus sign at configuration (5)). Note that the corresponding transitions are identified by the amplitude of the switches as determined from the fraction of material in the switching layer (see top left text inset of figure 2(a)). Overall the simulated blue line shows a good agreement with the experimental VSM data up to configuration (6). The IM model now fails to describe transition (6)–(7). This is due to the complex simultaneous switching (rearranging) of the three injector layers at this transition at 2520 Oe as derived from the experimental data which the simple IM model fails to capture [10, 24]. Due to this rearranging the subsequent transitions are predicted at the right field value but offset vertically up to and including configuration 9. For completeness a full description of the switching sequence as predicted by the IM model (blue solid line) can be found in figure S1 of the supplementary information (available at stacks.iop.org/Nano/25/105201/mmedia).

To overcome this shortcoming of the IM model we have artificially introduced the rearranging transition at 2520 Oe with amplitude $\Delta M/M_s = 0.182$ (see top left text inset of figure 2(a)) in the simulated red solid line. In the remainder of this paper we will indicate this artificially introduced transition with an exclamation mark as shown in figure 2(a). With this modification the IM simulation now correctly describes the amplitude and switching fields of the sequence (7)–(11). Note that the field at which the rearranging transition occurs happens before the bulk t_2 layers in the soliton propagation region (L6, L8, L10) switch (transitions (7)–(8), (8)–(9), (9)–(10) in figure 2(b)). This allows us to inject multiple solitons into the SL as we will present later.

In contrast to our former results [10], where H_c of the Pt/CoFeB/Pt layers was uniform for the whole SL, we find here that for Pt/Co, H_c increases from L6 upwards, up to a factor 3–4 for L10, to decrease to the same level as the bottom layers for L11 (see parameter list in figure 2(b)). The increasing H_c points to stronger domain wall pinning or delayed DW nucleation [23] in FM layers higher in the stack which indicates a change in microstructure, this is beyond the scope of this paper and a full study on the relation between the microstructure and the magnetic properties (J and H_c) will be published elsewhere.

3.2. Single soliton propagation

We define the polarity of a soliton by the magnetic orientation of the two layers forming the soliton when it straddles two layers coupled by J_2. At configuration (5) of figure 2(b) a soliton with negative polarity is injected between L3 and L4 as indicated by the blue minus sign. In figure 3 we show the propagation of this soliton through the SL using VSM. The field sequence used is shown in (a), in (b) we plot the corresponding normalized VSM signal as a function of time,
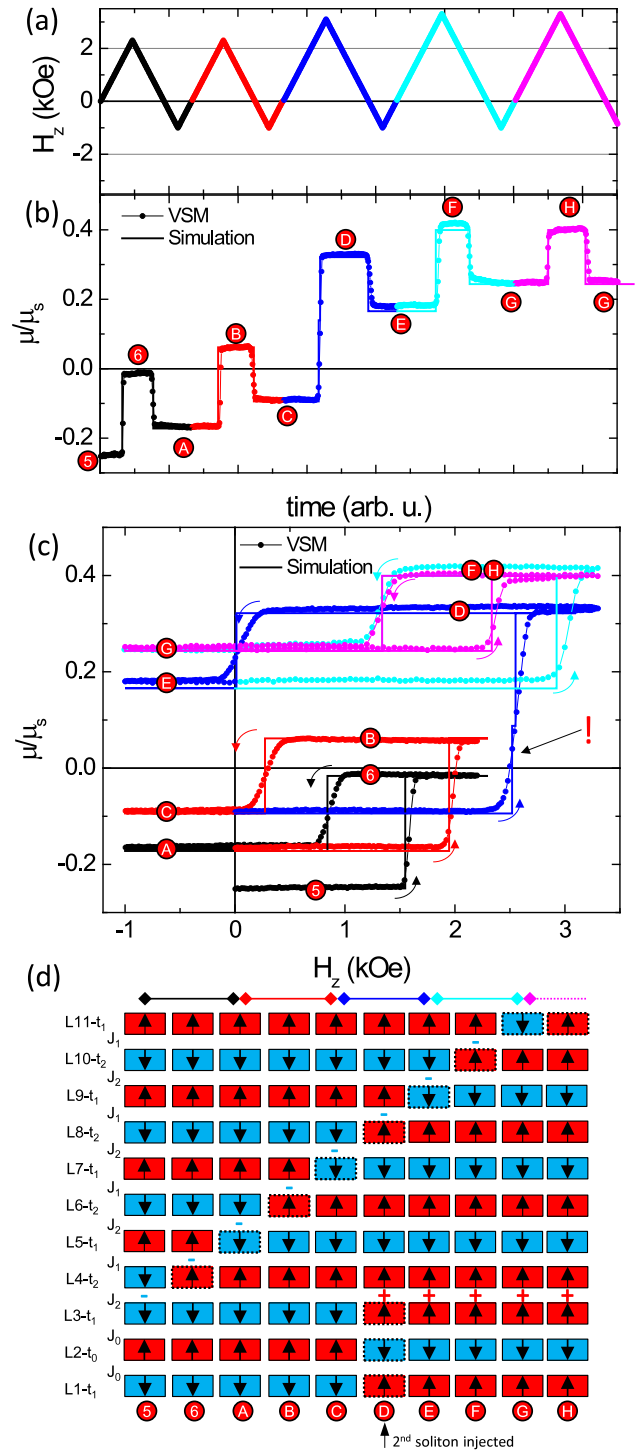

Figure 3. Synchronous propagation of a soliton with negative polarity up and out of the SL. (a) Triangular field cycle sequence used as a function of time. Corresponding normalized VSM magnetic moment as a function of time (b), as a function of applied field (c). The rearranging transitions have been indicated by the exclamation marks. (d) Schematic illustration of the magnetic configuration at each plateau in the VSM signal corresponding to the labeled balloons. The colored bars above the illustrations indicate the corresponding field cycle.

in (c) as a function of applied field and in (d) we schematically illustrate the SL configuration after every transition. The solid lines in (b) and (c) are simulated using the IM-model with the
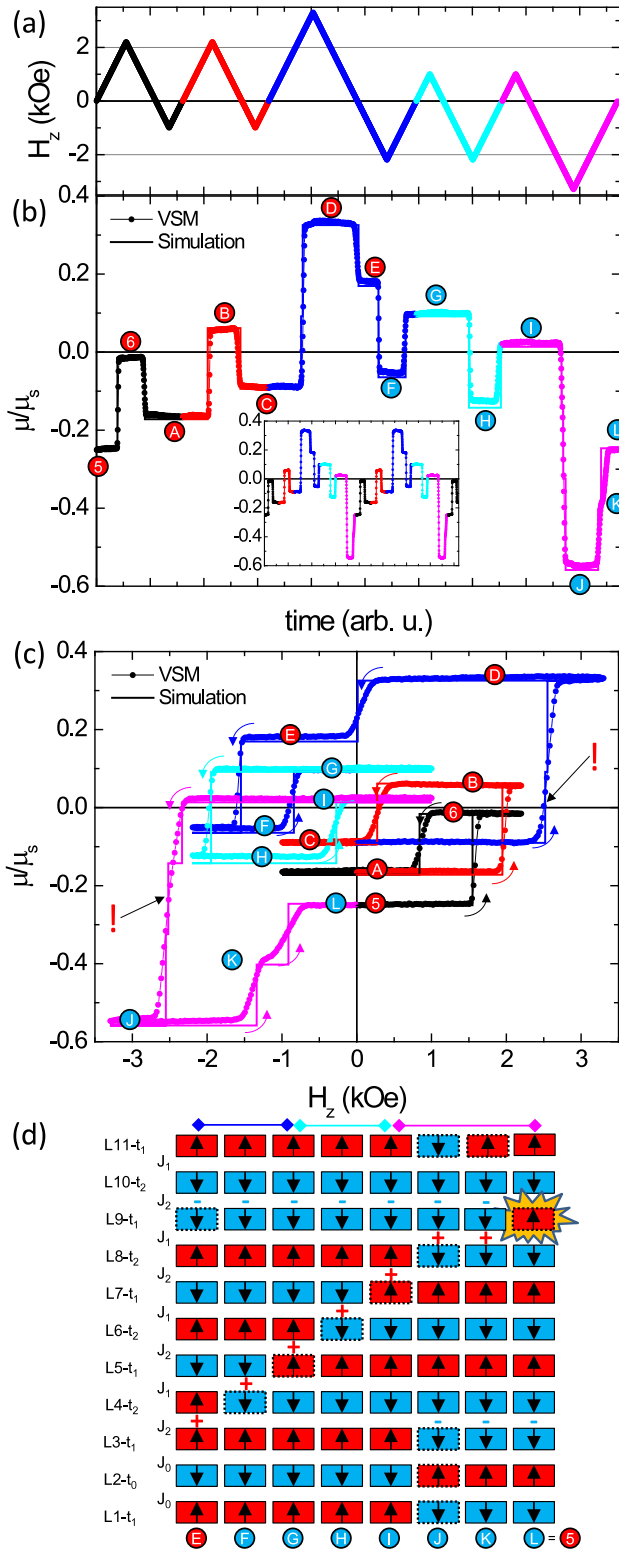
Figure 4. Propagation of two solitons with opposite polarity which annihilate at L9 when propagated into each other. (a) Triangular field cycle sequence used as a function of time. Corresponding normalized VSM magnetic moment as a function of time (b), as a function of applied field (c). The rearranging transitions have been indicated by the exclamation marks. (d) Schematic illustration of the magnetic configuration at each plateau in the VSM signal corresponding to the labeled balloons. The colored bars above the illustrations indicate the corresponding field cycle.

parameters as given in figure 2(b). The configurations labeled with numbered balloons are identical to the configurations shown in figure 2(b) and the letter labeled balloons identify the SL configuration given in figure 3(d). Before starting the measurement we prepare the SL in configuration (5) with a negatively polarized soliton between L3 and L4. We then start a triangular shaped field cycle (figure 3(a)) where every new cycle is given a different color. The switching fields at which the soliton propagates, H_{p1} and H_{p2} are given by [10]: $H_{p1} = H_c + (J_1 - J_2)/t_2$ and $H_{p2} = -H_c + (J_1 - J_2)/t_1$.

In the first field cycle (black) the soliton moves one layer up at H_{p1} where it now straddles two layers coupled by J_1. The field then decreases and at H_{p2} the soliton moves up another layer where it again straddles two layers coupled by J_2. The propagating soliton is identified by the increased normalized magnetic moment at remanence (A). This increase can be calculated as 0.3 nm of magnetic materials ($t_2 - t_1 = 0.9 - 0.6 = 0.3$ nm) has reversed its direction from a total of 7.7 nm Co in the stack, i.e. $\Delta M/M_s = (0.3/7.7) \times 2 = +0.078$, as observed. In the red field cycle the soliton again propagates two layers up (A)–(B) and (B)–(C). H_{p1}, however, has increased from 1548 Oe in the black field cycle (5)-(6) to 1947 Oe in the red field cycle (B)–(C). Also, H_{p2} (B)–(C) changes from 840 Oe in the black field cycle to 273 Oe in the red field cycle. This is mainly caused by the increase in H_c for layers up the SL and agrees with the equations given before. In the blue field cycle we need to further increase the amplitude of the applied field compared to the black and red field cycles to reach H_{p1}. We now, however, observe a large increase in total magnetic moment in the transition from configuration (C) to (D). In the experimental data, due to smearing of the transitions, the propagation of the soliton at field $H_{p1} = 1623 + (1158 - 322)/0.9 = 2552$ Oe coincides with the rearranging of the injector at 2520 Oe. The separation of these two switches can be seen by the two steps in the simulated curve of figure 3(c) (indicated by the exclamation mark as discussed before). On relaxing the field back to zero H_{p2} (D)–(E) occurs at 30 Oe. There are now two solitons in the stack, one with a positive polarity between L3 and L4 (red +), and the original soliton with negative polarity between L9 and L10 (blue −).

Positive (negative) fields propagate solitons with a negative (positive) polarity, provided that the amplitude of the driving field is large enough to reach $|H_{p1}|$. Therefore, we only propagate the negatively polarized soliton during the positive part of the cyan field cycle ((E)–(F) and (F)–(G)), which is thereby expelled out of the top of the SL. In the magenta field cycle the top layer flips back and forth (G)–(H) and (H)–(G) due to the expulsion of the soliton. In spite of the simplicity of the IM model the simulated curves describe the experimental data well.

This shows the basic propagation [10] and injection mechanism for sharp magnetic kink solitons of both polarities needed for a serial shift register.

3.3. Multiple soliton propagation and soliton annihilation

In figure 4 we show the propagation, injection and subsequent annihilation of two solitons as needed for logic operations. The
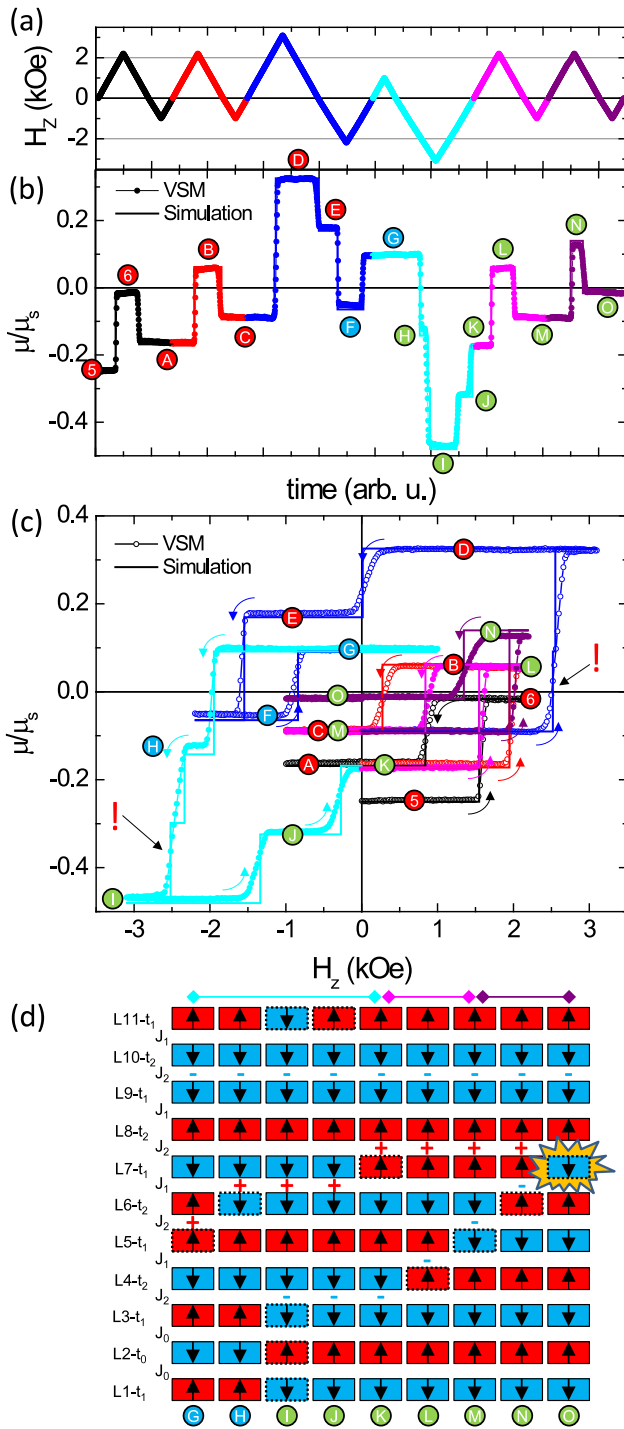
Figure 5. Injection of a third soliton and annihilation of two solitons in the bulk of the SL. (a) Triangular field cycle sequence used as a function of time. Corresponding normalized VSM magnetic moment as a function of time (b), as a function of applied field (c). The rearranging transitions have been indicated by the exclamation marks. (d) Schematic illustration of the magnetic configuration at each plateau in the VSM signal corresponding to the labeled balloons. The colored bars above the illustrations indicate the corresponding field cycle.

figure layout is identical to figure 3 and the numbering/lettering in the red balloons of figure 4 corresponds to the same SL configurations as given in figure 2(b) and 3(d). The blue

lettered balloons indicate new configurations. We start again with a soliton with negative polarity between L3 and L4 at (5). Using the same first three field cycles (black-red-blue) as in figure 4(a) (5)-(E), we propagate this soliton six layers up and in the process we inject a soliton with positive polarity between L3 and L4.

We are now in configuration (E). Instead of propagating the top soliton out of the SL as before, we propagate the positively polarized soliton upwards using negative applied fields. The propagation of the bottom soliton follows the exact same sequence as we have seen before in figure 3, albeit it now propagates on negative fields as expected. A propagating soliton with positive polarization is identified by a decrease in the magnetic moment. This brings us to configuration (I) after the cyan field cycle. At this point the two solitons with opposite polarization are spaced two layers apart. In the magenta field cycle we observe a large drop in magnetic moment at ∼−2400 Oe (I)–(J), this drop corresponds to three switching events taking place simultaneously due the thermal smearing of the transitions: (1) the switching of the top layer at −2335 Oe as it is aligned anti-parallel with the applied field, (2) rearranging of the injector at −2520 Oe injecting a negatively charged soliton, (3) the propagation of the positively charged soliton at −2552 Oe. In the simulated curve these individual three switches can be identified in the order described (the exclamation mark indicates the rearranging transition as discussed before). Note that there are now three solitons in the SL at configuration (J). As the field relaxes to zero first the top layer switches back and then the two oppositely polarized solitons at the top annihilate at L9, erasing them from the stack (K). We have now returned to the same configuration as we started with (L) = (5). Note that when two sharp kink solitons annihilate each other the anti-phase domain they separated is erased and no information of the former presence of the two solitons is left as is shown in column (L) of figure 4(d).

We can continue the same field cycle repeatedly as shown in the inset of figure 4(b), with the soliton propagation and injection fields occurring at the exact same fields (verified for ten full field cycles). This proves that the soliton propagation is not influenced by unsaturated nucleation embryos or asymmetric domain wall nucleation sites that might be left in the layers due to former field cycles [25] and/or solitons passing through. For future devices this indicates that the passing of multiple solitons does not alter the ratchet properties of the SL which is critical for true shift-register operation. Furthermore, the reproducible full annihilation of two solitons demonstrates that complex logic operations can be performed inside a shift register.

To complement the data on the annihilation operation of two solitons, we show in figure 5 the injection of a third soliton which we propagate to, and annihilate in the middle, of the SL. Figure 5 follows the same order and labeling conventions as introduced before. We start with the same fields cycles as used in figure 4 which brings us to configuration (G) (blue balloon). This is a stable state as both solitons are straddling a J_2 coupling. In the cyan field cycle we first propagate the positively polarized soliton one layer up (H) as before, but

instead of relaxing the field back to zero we increase it further to inject a negatively polarized soliton between L3 and L4 (I) (green balloon). As before, due to thermal smearing, the top layer also switches. On relaxing the applied field to zero, first the top layers switches back (J) and finally the positively polarized soliton propagates one layer up (K). Note that the SL now contains three solitons at stable positions. We then propagate the negatively polarized soliton we just injected four layers up in the magenta ((K)–(L) and (L)–(M)) and purple ((M)–(N) and (N)–(O)) field cycles where it annihilates at L7 with the positively polarized soliton. This effectively erases them both from the SL in the bulk, demonstrating the efficient annihilation of solitons in the bulk. From configuration (O) we can continue with injecting a positively polarized soliton by applying a negative field sufficient to rearrange the injector and repeat the whole sequence as before (not shown).

In an ideal SL with a homogenous H_c we would also have propagated the negatively polarized soliton between L9 and L10 in the magenta field cycle to be expelled out of the SL. However, the field required to propagate this soliton is too high (see figure 3(c)), i.e. the required field will switch the bulk layers lower in the SL, thereby erasing/repositioning solitons in the lower part of the SL (not shown). Hence, as discussed before, having a constant H_c for all layers up the SL, with the possibility to inject solitons, would allow for synchronous propagation of all the positive (negative) polarized solitons on negative (positive) applied fields.

This shows the basic ingredients for creating magnetic logic operations or instruction sets in SLs based on the spacing between and coding of information using the selective propagation of sharp magnetic kink solitons by their polarization.

3.4. Soliton–soliton interactions

From the simple nearest-neighbour IM model no soliton–soliton interactions are expected with the exception of the annihilation process. If the continuous film was patterned, the presence of long range dipolar interactions would introduce long range soliton–soliton interactions. This can be verified from our measurements as soliton–soliton interactions would manifest as a change in the propagation field when solitons approach each other. From analyzing the propagation fields in figures 3–5 we conclude that the propagation fields are similar in all cases within our measurement accuracy, i.e. the same absolute propagation fields are required to move regardless the presence or not of another soliton. For instance, H_{p1} and H_{p2} for a single soliton moving from L3–L4 to L4–L5 ((5)-(6) in figure 3) and then from L4–L5 to L5–L6 ((A)–(B) in figure 4) are identical to H_{p1} and H_{p2} measured when a soliton propagates through the same layers but in the presence of a soliton just above ((K)–(L) and (M)–(N) in figure 5).

4. Discussion

By symmetry, all the above soliton propagation and injection operations can be performed with inverted field cycles, the configurations are identical as shown albeit with every layer inverted (not-shown). Finally, different soliton injection strategies can be considered. For instance; by using spin-transfer- or spin-orbit-torque type of soliton injection strategies [26–30]. One could also combine different ferromagnetic materials in the same stack having intrinsically different H_c or, alternatively, irradiate the SL with ions in order to decrease the H_c of the top most layers and create a local injector at the top of the stack [31–35].

From a device perspective, the increasing H_{p1} for layers higher up in the stack is not wanted. Moreover, it forces us to modulate the applied field amplitude to propagate the soliton depending on where it is located in the stack. The increase in H_c indicates an underlying quality degradation of the layers as the SL grows. There is, however, much room for improvement by optimizing the growth conditions and/or using different materials. For instance, stronger domain wall pinning was observed before in pure Co compared to Boron doped Co and CoFeB [23, 31]. Indeed, in the Pt/CoFeB we used before we found a constant H_c for all layers in the SL [10]. We are, however, unable to inject multiple solitons using CoFeB/Pt with the used injection strategy (rearranging field of the injector). Hence, as a compromise we have used here Co/Pt, allowing us to inject multiple solitons at the cost of a dispersion in H_c. Speculatively, a higher magnetostriction of pure Co might explain the dependence of H_c on height in the SL compared to amorphous CoFeB. Furthermore, micromagnetic simulations taking the full magnetization reversal of the coupled layers into account, and systematically including different sources of domain wall nucleation/pinning sites and local anisotropy variations (for instance due to the aforementioned magnetostriction), might shed light on the observed dispersion in H_c and injector rearranging field value.

From logic point of view the soliton annihilation process is the XOR function if a 1 is represented by a soliton and a 0 by the absence of solitons. The way this can be done in a large SL with many solitons could be interpreted as an instruction pipeline in a microprocessor, i.e. the filling of the SL with oppositely polarized solitons spaced differently allows one to store an instruction set. These are simple examples but many others could be thought of using different magnetic logic coding schemes and/or algorithms [5].

5. Summary

We have demonstrated the injection, propagation and annihilation of multiple solitons in a SL which is a crucial step towards three-dimensional future memory and logic devices. All soliton manipulation processes could be repeated reproducibly showing full shift register and logic potential. Finally, as expected, we found no indication of soliton–soliton interactions within our experimental accuracy. The presented results show the highest level of logic operation ever performed on data in the magnetic state and brings closer the possibility of ultrahigh density three-dimensional all-magnetic microprocessors.

6. Methods

The samples are fabricated by DC magnetron sputtering using an Ar pressure of 7.5×10^{-3} mbar in a vacuum system

with a base pressure of $\sim 3 \times 10^{-8}$ mbar. All samples are prepared on precut Si substrates ($\sim 1 \times 1$ cm^2) with a native oxide layer. The substrates were cleaned by acetone and isopropanol in an ultrasound bath. For Ta, Co and Ru DC magnetron powers of 50, 60, 100 W were used, respectively. The growth rates were calibrated to 0.059 (Ta), 0.049 (Co), 0.126 (Ru) nm s^{-1} by atomic force microscopy on step edges with an estimated error margin of 10%. For Pt we used 100 W (0.215 nm s^{-1}) for the buffer and capping layers and 30 W (0.063 nm s^{-1}) for the interlayers. During deposition the substrates were rotated (20 rot min^{-1}) and the layer thicknesses were controlled by timing the opening of shutters with a 1 ± 0.25 s time resolution. These are the same growth conditions as used in our previous report (Pt/CoFeB based ratchet [10]). Polar magneto-optical Kerr effect (MOKE) and vibrating sample magnetometery (VSM) at room temperature are used to determine the magnetic properties of the samples. The magnetic field is always applied perpendicular to the film plane.

Acknowledgments

Author Contributions

RL and RC planned the experiment; RL fabricated the samples, performed the soliton experiments and wrote the manuscript; RL and DCMCP analyzed the data. All authors discussed the results and contributed to the scientific interpretation as well as to the writing of the paper.

References

[1] Allwood D A *et al* 2005 Magnetic domain-wall logic *Science* **309** 1688–92

[2] Cowburn R P and Welland M E 2000 Room temperature magnetic quantum cellular automata *Science* **287** 146–1468

[3] Wolf S A *et al* 2001 Spintronics: a spin-based electronics vision for the future *Science* **294** 1488–95

[4] Chappert C, Fert A and Nguyen van Dau F 2007 The emergence of spin electronics in data storage *Nature Mater.* **6** 813–23

[5] Niemier M T *et al* 2011 Nanomagnet logic: progress toward system-level integration *J. Phys.: Condens. Matter* **23** 493202

[6] Parkin S S P, Hayashi M and Thomas L 2008 Magnetic domain-wall racetrack memory *Science* **320** 190–4

[7] Kawahara T, Ito K, Takemura R and Ohno H 2012 Spin-transfer torque Ram technology: review and prospect *Microelectron. Reliab.* **52** 613–27

[8] Baryakhtar V G, Chetkin M V, Ivanov B A and Gadetskii S N 1994 *Dynamics of Topological Magnetic Solitons: Experiments and Theory* vol 129 (Berlin: Springer)

[9] Wang R W, Mills D L, Fullerton E E, Mattson J E and Bader S D 1994 Surface spin-flop transition in Fe/Cr(211) superlattices—experiment and theory *Phys. Rev. Lett.* **72** 920–3

[10] Lavrijsen R *et al* 2012 Magnetic ratchet for 3-dimensional spintronic memory and logic *Nature* **494** 647–50

[11] Micheletti C, Griffiths R B and Yeomans J M 1999 Surface spin-flop and discommensuration transitions in antiferromagnets *Phys. Rev. B* **59** 6239–49

[12] Sbiaa R, Meng H and Piramanayagam S N 2011 Materials with perpendicular magnetic anisotropy for magnetic random access memory *Phys. Status Solidi RRL* **5** 413–9

[13] Åkerman J 2005 Toward a universal memory *Science* **308** 508–10

[14] Parkin S S P 1991 Systematic variation of the strength and oscillation period of indirect magnetic exchange coupling through the 3d, 4d and 5d transition metals *Phys. Rev. Lett.* **67** 3598–601

[15] Bruno P 1995 Theory of interlayer magnetic coupling *Phys. Rev. B* **52** 411–39

[16] Li X X, Bao J, Xu X-G and Jiang Y 2008 Oscillatory antiferromagnetic interlayer coupling in CoPt multilayer with perpendicular anisotropy *Solid State Commun.* **148** 209–12

[17] Lavrijsen R *et al* 2012 Tuning the interlayer exchange coupling between single perpendicularly magnetized CoFeB layers *Appl. Phys. Lett.* **100** 052411

[18] Hellwig O, Berger A, Kortright J B and Fullerton E E 2007 Domain structure and magnetization reversal of antiferromagnetically coupled perpendicular films *J. Magn. Magn. Mater.* **319** 13–55

[19] Vaz C A F, Bland J A C and Lauhoff G 2008 Magnetism in ultrathin film structures *Rep. Prog. Phys.* **71** 056501

[20] Johnson M, Bloemen P, den Broeder F and de Vries J 1996 Magnetic anisotropy in metallic multilayers *Rep. Prog. Phys.* **59** 1409

[21] Hayashi M, Thomas L, Moriya R, Rettner C and Parkin S S P 2008 Current-controlled magnetic domain-wall nanowire shift register *Science* **320** 209–11

[22] Kim K-J *et al* 2010 Electric control of multiple domain walls in Pt/Co/Pt nanotracks with perpendicular magnetic anisotropy *Appl. Phys. Express* **3** 083001

[23] Lavrijsen R *et al* 2010 Reduced domain wall pinning in ultrathin Pt/Co$_{100-x}$B$_x$/Pt with perpendicular magnetic anisotropy *Appl. Phys. Lett.* **96** 022501

[24] Metaxas P J *et al* 2010 Dynamic binding of driven interfaces in coupled ultrathin ferromagnetic layers *Phys. Rev. Lett.* **104** 237206

[25] Iunin Y L *et al* 2007 Asymmetric domain nucleation and unusual magnetization reversal in ultrathin Co films with perpendicular anisotropy *Phys. Rev. Lett.* **98** 117204

[26] Ralph D C and Stiles M D 2008 Spin transfer torques *J. Magn. Magn. Mater.* **320** 1190

[27] Liu L, Pai C-H, Tseng H W, Ralph D C and Buhrmann R A 2012 Spintorque switching with the giant spin Hall effect of tantalum *Science* **336** 555

[28] Tudosa I, Katine J A, Mangin S and Fullerton E E 2010 Perpendicular spintorque switching with a synthetic antiferromagnetic reference layer *Appl. Phys. Lett.* **96** 212504

[29] Sipr O, Minar J, Mankovsky S and Ebert H 2008 Influence of composition, many-body effects, spinorbit coupling, and disorder on magnetism of CoPt solid-state systems *Phys. Rev.* B **78** 144403

[30] Katine J A and Fullerton E E 2008 Device implications of spin-transfer torques *J. Magn. Magn. Mater.* **320** 1217–26

[31] Lavrijsen R, Franken J, Kohlhepp J, Swagten H and Koopmans B 2010 Controlled domain-wall injection in perpendicularly magnetized strips *Appl. Phys. Lett.* **96** 222502

[32] Warin P *et al* 2001 Modification of Co/Pt multilayers by gallium irradiationpart 2: the effect of patterning using a highly focused ion beam *J. Appl. Phys.* **90** 3850–5

[33] Adam J P *et al* 2012 Magnetization reversal by confined droplet growth in soft/hard hybrid nanodisks with perpendicular anisotropy *Phys. Rev.* B **85** 214417

[34] Chappert C *et al* 1998 Planar patterned magnetic media obtained by ion irradiation *Science* **280** 1919

[35] Hellwig O *et al* 2009 Coercivity tuning in Co/Pd multilayer based bit patterned media *Appl. Phys. Lett.* **95** 232505